On the Transition from AGB Stars to Planetaries: The Spherical Case

Detlef Schönberner and Matthias Steffen
Astrophysikalisches Institut Potsdam, An der Sternwarte 16,
D-14482 Potsdam

Abstract. We discuss the basic physical model and the relevant processes responsible for creating and shaping planetary nebulae out of a cool AGB wind envelope. We show that a hydrodynamical treatment along the upper AGB leads quite naturally to more realistic starting configurations for planetaries with density slopes steeper than r^{-2} . Taking into account photoionization and wind interaction in a realistic manner, the hydrodynamics of post-AGB wind envelopes leads to density structures and velocity fields in close resemblance to observations of spherical or elliptical planetary nebulae.

1. Introduction

Although we are here only interested in an explanation of non-spherical structures observed so often in planetary nebulae (PN), a detailed study of spherical systems appears to be important for at least two reasons. The first is a more physical one and refers to our still rather poor knowledge of PN formation and evolution. The use of spherical models allows a detailed study of basic physical processes without having to worry about influences caused by non-spherical structures. The other reason is a technical one: the presently available computing power is too limited to follow the evolution of non-spherical model planetaries over their whole life with sophisticated physics and good spatial resolution.

It is expected that basic physical processes work similarly in systems with a complex geometry. They set the stage for the other phenomena responsible for the development of non-spherical structures and should always be considered.

2. The Basic Physical System

The evolution of an AGB star is driven by mass loss until the mantle is lost and the remnant begins to contract rapidly towards higher temperatures. Eventually the burning shells extinguish and the white dwarf cooling path is reached. The remnant's luminosity and evolutionary speed depend very sensitively on its mass, and possible ranges of luminosity and speed are shown in Fig. 1. All these remnants stem from different progenitors whose evolutionary histories have been consistently followed from the main sequence through all the later phases including mass loss and thermal pulses (see Blöcker 1995 for the details). Similar computations have been performed by Vassiliades & Wood (1994).

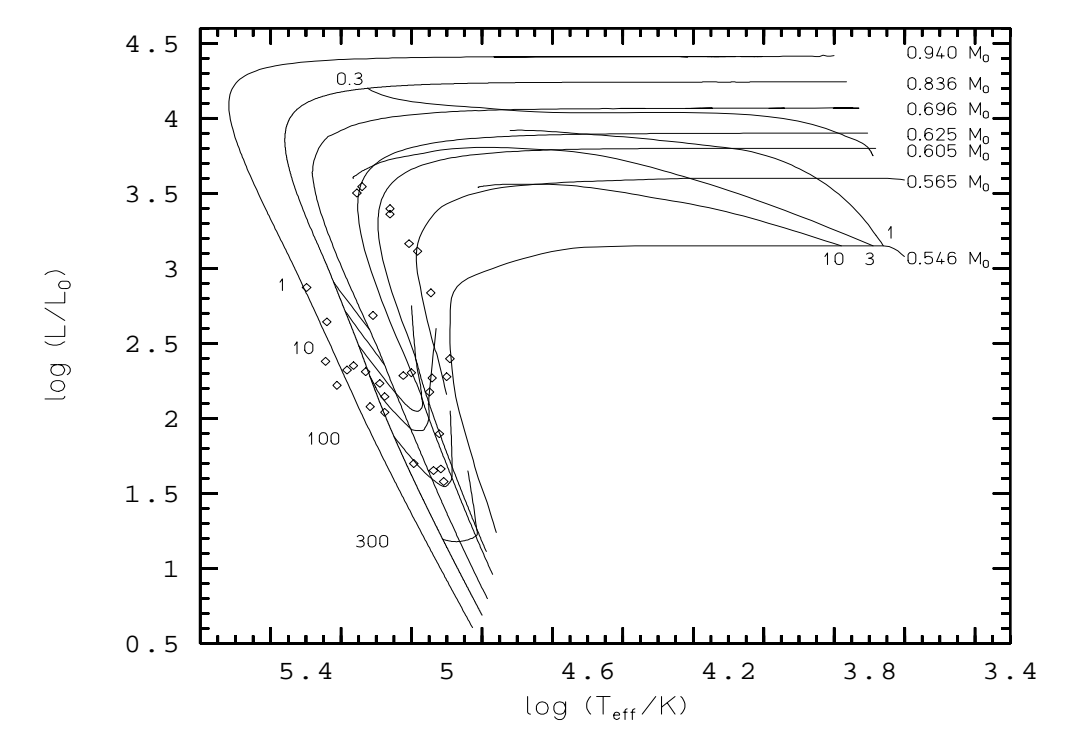


Figure 1. Evolutionary tracks of hydrogen-burning post-AGB models with isochrones (in 10³ yrs), together with a sample of central stars of 'optically thick' PNe, from Blöcker (1995). The post-AGB ages are counted from positions close to the AGB and may depend on the assumed mass-loss rates in the vicinity of the AGB (cf. Blöcker 1995).

The evolution of the AGB remnant, - the central star -, in temperature and luminosity drives in turn the development of a PN out of a cool wind envelope by two processes, viz. by the concomitant changes of the stellar radiation field and wind power. The relative importance of both processes with respect to the evolution of a planetary varies with the central-star's age (or effective temperature). The number of hydrogen-ionizing photons emitted per second increases rapidly with the remnant's effective temperature, but later the luminosity decrease starts to dominate. For a typical central-star mass of 0.6 $\rm M_{\odot}$ the maximum flux of ionizing photons occurs between 60 000 and 70 000 K. The very rapid luminosity drop after the central star has reached its maximum effective temperature (cf. Fig. 1) may cause substantial recombination. It is important to follow this late evolutionary phase with a fully time-dependent code that treats all the relevant physical processes, i.e. ionization, recombination, heating and cooling (Marten 1995).

The property of mass-loss during the post-AGB evolution is more difficult to evaluate. For an AGB star we have winds driven by radiation pressure on small grains with momentum transfer to the gas. The outflow rates depend on the star's luminosity and effective temperature (cf. Sedlmayr & Dominik 1995; Arndt, Fleischer, & Sedlmayr 1998). Typical rates are between about 10^{-7} and

 $10^{-4}~{\rm M}_{\odot}$, with outflow velocities from 5 to 25 km/s, i.e. $\lesssim V_{\rm esc}$, the surface escape velocity. During the post-AGB contraction, mass-loss rates are lower by orders of magnitude, but the wind velocities are substantially higher. The driving of the outflow occurs via radiation pressure on lines (cf. Pauldrach et al. 1988), $\dot{M} \simeq 1.3 \cdot 10^{-15} \, (L/L_{\odot})^{1.86}$, and typical values are $\approx 10^{-8} \, {\rm M}_{\odot}/{\rm yr}$ for the rate, but now with $V \simeq 1\,000\ldots 10\,000$ km/s $\simeq (2\ldots 4)V_{\rm esc}$. The wind power, $P = \dot{M}V^2/2$, reaches its maximum close to the turn-around point at maximum effective temperature and declines then rapidly with the luminosity.

It should, however, be noted that the stellar wind does not interact directly with the nebular/AGB material. Instead, the wind's kinetic energy thermalizes through a shock and adds to the energy and matter content of hot, shocked wind material emitted at earlier times. The thermal pressure of this 'bubble' of hot but very tenuous gas drives the inner edge of the planetary. Though it is actually the time integral over the wind power that determines the energy content of the bubble, the maximum bubble pressure coincides roughly with the maximum wind power of the central star.

3. Formation and Evolution of PN

Given typical mass-loss rates between 10^{-5} and $10^{-4}~{\rm M_{\bigodot}/yr}$ during the final AGB evolution and the still rather low wind velocities during the remnant's transition through the cool part of the Hertzsprung Russell diagram, the dynamical effects of wind interaction are expected to be modest. As soon as the remnant becomes sufficiently hot, ionization sets in and gives birth to a HII region deeply embedded in the neutral/molecular circumstellar AGB material. Thermal pressure of the ionized matter drives a shock wave into the ambient slow material, and the front itself defines the outer edge, $R_{\rm pn}$, of the new PN even if the ionization has already broken through into the surrounding region. The front's speed, $R_{\rm pn}$, is mainly determined by the balance of the shell's thermal pressure with the ram pressure exerted by the ambient matter. At a given time, speed and position of the outer rim of a planetary depend thus on the mass-loss history over the last 10 000 to 20 000 years of AGB evolution. The mass embraced by $R_{\rm pn}$ is steadily growing with time at the expense of the still undisturbed (although possibly ionized) AGB wind material. We emphasize here that $R_{\rm pn}$ is not a matter velocity and cannot be observed spectroscopically!

As outlined in Sect. 2. above, the wind interaction through the hot bubble becomes more and more important with time and compresses and accelerates the inner parts of the shell into a high-density shell, the so-called 'rim' (cf. Balick 1987). Since the bubble's pressure is controlled by the central-star's wind properties, the evolution of the central star controls the shaping of the inner parts of a planetary.

Hydrodynamical simulations that took ionization and wind interaction properly into account have shown that both effects lead unavoidably to typical double-shell structures consisting of an inner high-density 'rim' surrounded by a low-density 'shell' with no resemblance to the initial density and velocity distributions (cf. Marten & Schönberner 1991; Mellema 1994). Thus planetaries do not contain direct information on precedings mass-loss phases during the end of the AGB evolution!

4. Two-Component Radiation Hydrodynamics Simulations of the Final AGB Phase

Attempts to model the evolution of planetary nebulae face the problem of selecting the proper initial configuration, i.e. density distribution and velocity field. Since practically nothing is known, rather simple conditions are usually assumed, viz. mass outflow with constant speed and rate. Our present knowledge of the late stages of stellar evolution allows, however, to draw more detailed conclusions: (i) The theory of radiation-driven winds on the AGB suggests that both the outflow rate and -speed depend on the stellar luminosity and effective temperature, and on the chemical composition as well (Arndt et al. 1997). (ii) Stellar evolution theory predicts large luminosity variations (up to a factor three) during thermal pulses, expected to lead to drastic variations of outflow rates and speeds.

One can expect that hydrodynamical simulations of AGB wind envelopes along the upper AGB give very useful informations about initial conditions to be expected for planetaries. A first step into this direction has been reported by Schönberner et al. (1997). The stellar outflow is assumed to be spherically symmetric, and the equations of hydrodynamics are solved for the gas and the dust component, coupled by momentum exchange due to dust-gas collisions. We used a modified version of the code developed by Yorke & Krügel (1977), making use of the following simplifications: (i) Radiation transfer is considered only for the dust component, i.e. exchange of photons between dust grains and the gas is neglected. (ii) The dust temperature is computed from radiative equilibrium, and the gas (neutral hydrogen) is assumed to have the same (local) temperature. (iii) The dust consists of single-sized grains, either based on oxygen or carbon chemistry, adopting a fixed dust-to-gas ratio at the dust condensation point.

We introduced time-dependent values of stellar mass, luminosity, effective temperature and variable mass loss (as shown in Fig. 2) with a constant flow velocity equaling the local sound speed, ≈ 3 km/s as a boundary condition. The radiation pressure on the grains and the momentum transfer to the gas leads to an acceleration of the material to typical final outflow velocities around 10 to 15 km/s, in agreement with observations. A more detailed description of this fully implicit radiation hydrodynamics code has been given by Steffen et al. (1997) and Steffen, Szczerba, & Schönberner (1998).

4.1. Evolution through the Upper AGB and Beyond

We extended our AGB hydrodynamical simulations somewhat into the post-AGB regime, using the mass-loss prescription shown in the upper panel of Fig. 2. Mass-loss rate and effective temperature (or radius) of the star are coupled according to the prescription of Blöcker (1995), and the most prominent feature is a rapid decrease of the rate by orders of magnitude within about 100 years around effective temperatures of 6 000 K. The consequence is a rapid detachment and thinning of the dust shell since the density of any newly formed dust is strongly reduced and gives no detectable signature. This is illustrated by the sequence of spectral energy distributions in the lower panel of Fig. 2 which covers a time interval of less than 500 years. For this simulation we adopted an oxygen-based grain type ("Astronomical Silicates"), and the gradual disappearance of

the strong silicate absorption feature with increasing shell detachment is clearly seen. At the same time, the previously totally obscured AGB remnant becomes visible. Our modelled spectral energy distributions resemble very much those of known proto-planetary nebulae (Hrivnak, Kwok, & Volk 1989), indicating that the mass-loss variations at the end of the AGB evolution as chosen by Blöcker (1995) are close to reality!

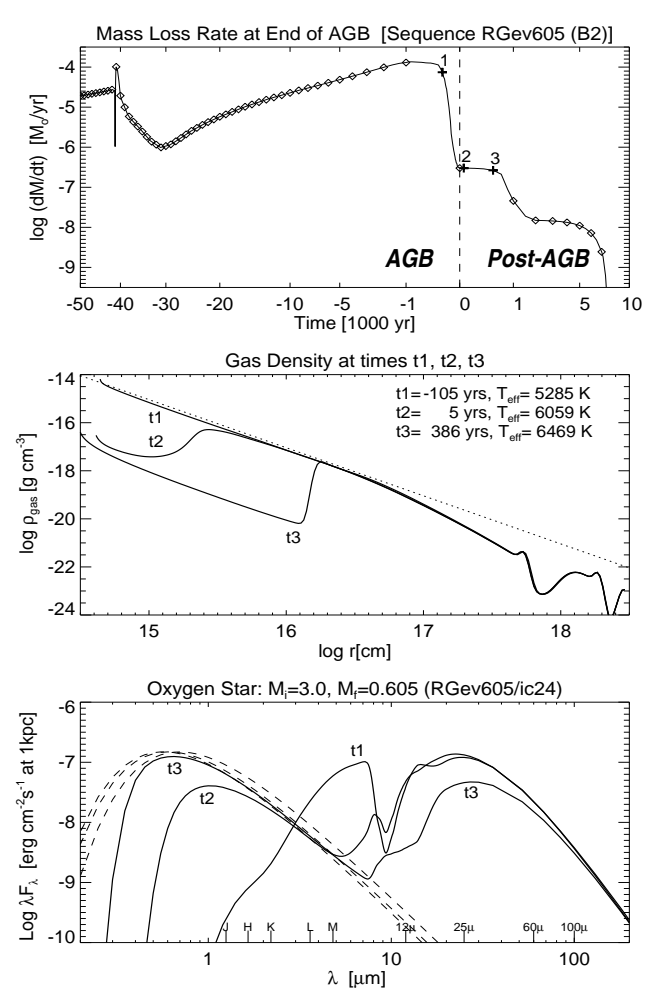


Figure 2. **Top:** Adopted mass-loss rate for the late AGB and early post-AGB evolution ending up with a remnant of $0.605~\mathrm{M}_{\odot}$ (Blöcker 1995). **Middle:** Radial gas density distributions for models with silicate grains at the three selected times marked in the upper panel. **Bottom:** Spectral energy distributions at the same times. The dashed lines are the corresponding intrinsic spectra of the central star.

Due to the variations of the mass-loss rate as shown in the upper panel of Fig. 2, the density structure is clearly different from the usual assumption of a $\rho \propto r^{-2}$ law (middle panel): The density dip near $r = 10^{18}$ cm is caused by the last thermal pulse about 30 000 years ago (cf. upper panel), while the rapid density increase towards the inner parts of the shell ($\rho \propto r^{-3}$) is due to the

recent increase of mass-loss rate. Further inwards the density increase flattens somewhat $(\rho \propto r^{-1})$. The outflow velocity is rather constant, ≈ 11 km/s, except for a slight decrease during the last thermal pulse.

4.2. Evolution across the Hertzsprung Russell Diagram

Little is really known about the development of wind strength and speed during the early post-AGB evolution. In the model shown in Fig. 2 the mass loss is set to the Reimers prescription (Reimers 1977) which is then kept until the remnant becomes hot enough for the theory of radiation driven winds to be applicable (Pauldrach et al. 1988). A more detailed description how mass-loss rate and wind speed may vary in the course of the post-AGB evolution is given in Marten & Schönberner (1991).

In order to investigate the transformation of a cool AGB wind envelope into a planetary nebula, we used the model structure shown in Fig. 2 at time t2 as input for another radiation hydrodynamics code. This one-component explicit code is based on a second-order Godunov-type advection scheme and considers time-dependent ionization, recombination, heating and cooling of six elements (H, He, C, N, O, Ne) with all of their ionization stages. More details can be found in Perinotto et al. (1998).

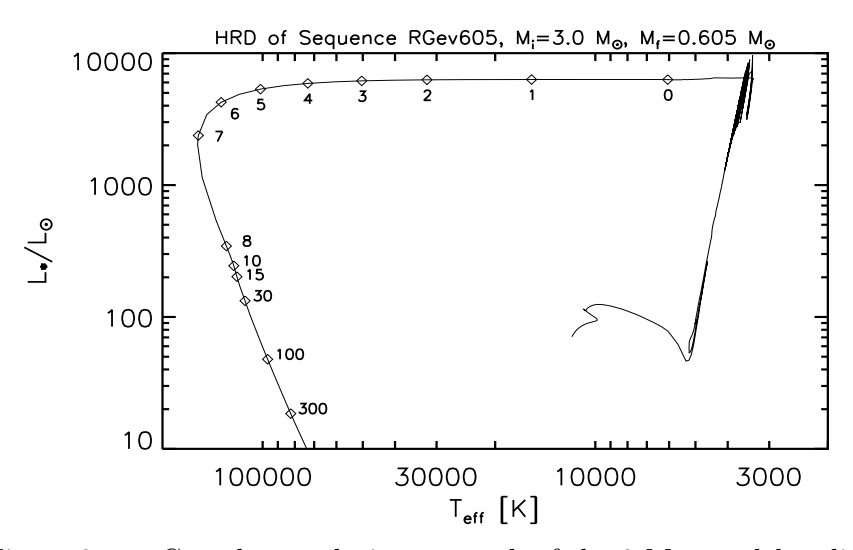


Figure 3. Complete evolutionary track of the 3 $\rm M_{\odot}$ model ending up as a 0.605 $\rm M_{\odot}$ white dwarf as used in our numerical simulations (from Blöcker 1995). Time marks (in 10^3 yrs) along the post-AGB path correspond to the post-AGB time scale given in Fig. 2.

A visualization how our model planetary develops in size, brightness and structure is presented in Fig. 4, showing $H\alpha$ surface-brightness distributions for selected models taken from our hydrodynamical simulation along the post-AGB evolutionary path displayed in Fig. 3.

At age = 1837 yrs (upper left in Fig. 4) ionization has already created a small but bright shell limited by a density wave which keeps the photons trapped. The peak flow velocity in this wave is 23 km/s, whereas the flow at the inner

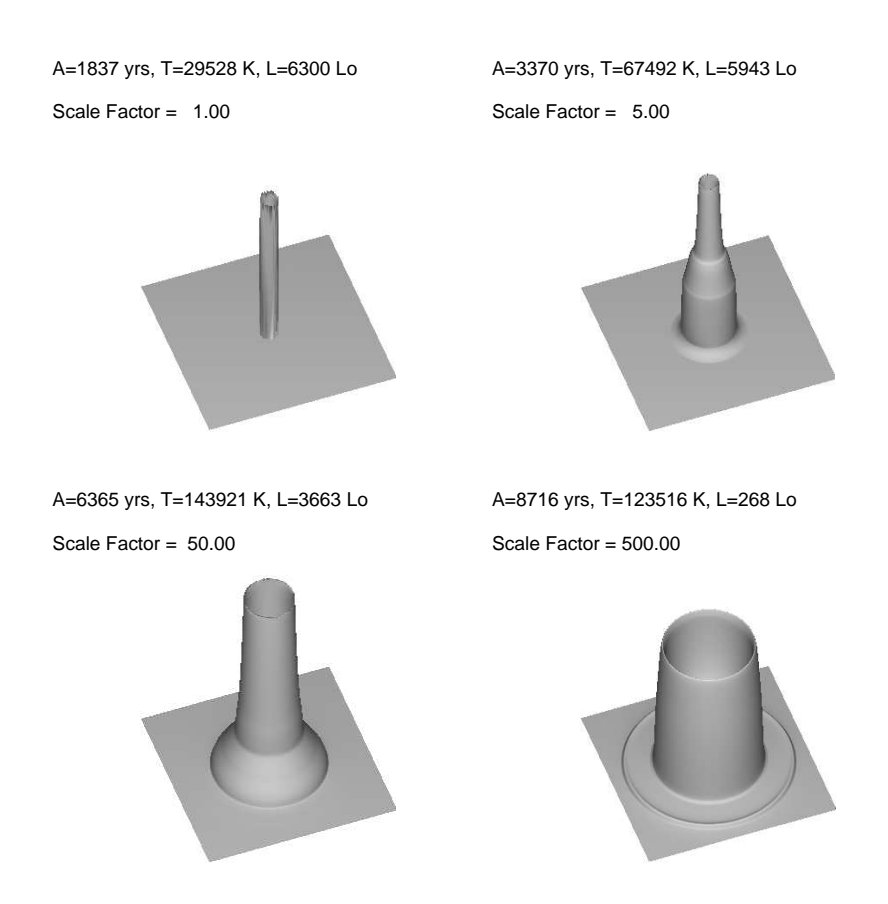


Figure 4. 3D representation of the surface-brightness distributions in $H\alpha$ of selected models along the post-AGB track displayed in Fig. 3. The models are labelled by their post-AGB age, effective temperature and luminosity of their central stars. Scale factors were applied in order to compensate for the decrease of the surface brightness with time.

edge of the shell is nearly stalling with only about 4 km/s. About 1500 years later (upper right) the ionization has broken through the shock, and the shell expands and dilutes because the wave front (the shock) is further accelerated due to the steeper than ρ^{-2} density slope. At about this time, wind interaction becomes noticeable through the formation of a compressed, bright 'rim' at the inner edge of the shell.

At age = 6365 yrs (lower left), the brightness contrast between inner rim and shell has significantly increased by the combined action of the shell's expansion into the AGB wind and compression from inside by the 'hot bubble'. The whole structure corresponds to a typical 'attached-halo multiple-shell PN' (Stanghellini & Pasquali 1995). The maximum flow velocity, immediately behind the shock front, is now 32 km/s, that of the rim matter about 24 km/s. This model agrees also qualitatively with the results of a structural and kinematical study of Gesicki, Acker, & Szczerba (1996) who found, e.g., for the double-shell

planetary IC 3568 shell velocities up to 40 km/s, but only about 10 km/s for the inner dense parts (the rim).

When the central star's luminosity has dropped rapidly to only a few $100~\rm L_{\odot}$, recombination within the shell reduces its brightness to typical halo values (age = 8716 yrs, lower right) which ends then the double shell phase that lasted from about age = 2800 till age = 7600 yrs, i.e. for a quite substantial fraction of a typical PN life time. Though the shell's brightness compares now with that of a halo, it is not a halo: the matter within the recombined shell continues to expand and compresses the AGB gas into a dense but thin shell, leading to substantial limb brightening. An example for such a structure is NGC 2438 which consists of a bright ring-like shell surrounded by a limb-brightened 'halo'. The analysis of Corradi et al. (in preparation) shows that this 'halo' is actually the recombined former shell set up by ionization at the very beginning of the planetary's life.

References

Arndt, T. U., Fleischer, A. J., & Sedlmayr, E. 1997, A&A, 327, 614

Balick, B. 1987, AJ, 94, 671

Blöcker, T. 1995, A&A, 297, 727

Gęsicki, K., Acker, A., & Szczerba, R. 1996, A&A, 309, 907

Hrivnak, B. J., Kwok, S., & Volk, K. 1989, ApJ, 346, 265

Marten, H. 1995, in Annals of the Israel Physical Society Vol. 11, Asymmetrical Planetary Nebulae, ed. A. Harpaz & N. Soker, 273

Marten, H., & Schönberner, D. 1991, A&A, 248, 590

Mellema, G. 1994, A&A, 290, 915

Pauldrach, A., Puls, J., & Kudritzki, R.-P., Méndez, R. H., & Heap, S. H. 1988, A&A, 207, 123

Perinotto, M., Kifonidis, K., Schönberner, D., & Marten, H. 1998, A&A, 332, 1044

Reimers, D. 1977, in Problems in Stellar Atmospheres and Envelopes, ed. B. Baschek, W. H. Kegel, & G. Traving (Berlin: Springer), 229

Schönberner, D., Steffen, M., Stahlberg, J., Kifonidis, K., & Blöcker, T. 1997, in Advances in Stellar Evolution, ed. R. T. Rood & A. Renzini (Cambridge: University Press), 146

Sedlmayr, E., & Dominik, C. 1995, Ap&SS, 73, 211

Stanghellini, L., & Pasquali, A. 1995, ApJ, 452, 286

Steffen, M., Szczerba, R., & Schönberner, D. 1998, A&A, 337, 149

Steffen, M., Szczerba, R., Menshchikov, A., & Schönberner, D. 1997, A&AS, 126, 39

Vassiliades, E., & Wood, P. R. 1994, ApJS, 92, 125

Yorke, H. W., & Krügel, E. 1977, A&A, 54, 183